

Supplementary Information

A dual-function probe with aggregation-induced emission feature for Cu²⁺ detection and chemodynamic therapy

Juan Fu^{a,#}, Xin Hu^{a,#}, Teng Guo^a, Weifeng Zhu^b, Jianwen Tian^a, Meiyong Liu^{a,b,*}, Xiaoyong Zhang^{a,*}, Yen Wei^{c,d,*}

^a Department of Chemistry, Nanchang University, 999 Xuefu Avenue, Nanchang 330031, China.

^b Key Laboratory of Modern Preparation of TCM, Ministry of Education, Jiangxi University of Traditional Chinese Medicine, Nanchang 330004, China

^c Department of Chemistry and the Tsinghua Center for Frontier Polymer Research, Tsinghua University, Beijing, 100084, P. R. China.

^d Department of Chemistry and Center for Nanotechnology and Institute of Biomedical Technology, Chung-Yuan Christian University, Chung-Li 32023, Taiwan

These authors are contributed equally to this work

1 Experimental

1.1 Analytical instruments

¹H nuclear magnetic resonance (NMR) and ¹³C NMR spectra were recorded on a Bruker AM 400 spectrometer (400 MHz, Bruker Co, Germany) and CDCl₃ was the solvent. ESI-MS spectral data were recorded on a hybrid quadrupole-TOF mass spectrometer (UHPLC30A-Trip TOFTM 5600, SCIEX, USA). The Fourier transform infrared (FT-IR) spectra were measured on a Nicolet5700 (Thermo Nicolet corporation). The UV-visible absorption spectra were collected with a Perkin Elmer LAMBDA 35 UV/vis system (Perkin Elmer Life and Analytical Sciences, Shelton, USA) using quartz cuvettes of 1 cm path length. The fluorescence spectral data were recorded with a fluorescence spectrophotometer (Perkin Elmer LS55, Massachusetts, USA) with a slit width of 7 nm for both excitation and emission. The dynamic light scattering (DLS) was measured via Zetasizer Nano ZS90 (Malvern Instruments Ltd., Worcestershire, UK). The fluorescence quantum yield and fluorescence lifetime of TPACP in mixture of DMSO/water (1:9) were measured using fluoroSENS instrument (Gilden Photonics). The size and morphology of those as-prepared samples were characterized by transmission electron microscope (TEM) (Hitachi 7650B microscope operating at 80 kV). The scanning electron microscopy (SEM) images were used to view the material structure with environmental scanning electron microscope (ESEM, FEI 123 Quanta250) (FEI Co., LTD, USA). X-ray photoelectron spectroscopy (XPS) was provided by the VGESCALAB 220-IXL spectrometer. Cell imaging was conducted on confocal laser scanning microscope (CLSM, Zeiss 710 3-channel, Germany).

1.2 Materials and solvents

Unless otherwise noted, all reagents were obtained from commercial suppliers and were used as received without further purification. 4-(Diphenylamino)phenylboronic acid, 4-bromo-2-hydroxybenzaldehyde, diethylmalonate, 2-(aminomethyl)pyridine, 4-(dimethylamino)pyridine (DMAP), tetrakis(triphenyl phosphine)palladium(0), 1-Ethyl-3-(3-dimethylaminopropyl)carbodiimide hydrochloride (EDCI) were purchased from Heowns Biochemical Technology Co., Ltd. (Tianjin, China). Analytical reagent grade solvents, such as tetrahydrofuran (THF), dimethylsulfoxide (DMSO), dichloromethane (DCM), ethyl acetate (EtOAc), Petroleum ether (PE), ethanol, piperidine, chloroform, NaOH and hydrochloric acid were bought from Damao Chemical Reagent Factory (DM). All the metal ions used are standard solution of metal ions from Aladdin Industrial Co. Ltd. (Shanghai, China). Furthermore, monitoring of the reaction's progress was performed with F254 thin layer chromatography

(TLC) and visualization of the components was achieved via observation under UV light (365 nm).

1.3 General procedure for the synthesis of compounds

1.3.1 General preparation of compound 1

Compound 1 was synthesized based on previous work¹.

1.3.2 General preparation of compound 2

A solution of compounds 1 (2.4 g, 6.6 mmol) and diethyl malonate (1.06 g, 6.6 mmol) in EtOH (30 mL) was treated with piperidine (2.2 mL) and glacial acetic acid (2 drops). The reaction mixture turned from yellow to orange. The reaction was continued to start at 80 °C for 5h. After completion of reaction, ethanol was evaporated. The residue was dissolved in HCl (2 M) and extracted with ethyl acetate. The organic layer was washed with water, brine and dried over anhydrous sodium sulfate. The crude product was purified by silica-gel column chromatography using ethyl acetate/petroleum ether (1/6) as the eluent to obtain compound 2 as yellow solid (1.6 g, 52.6%). ¹H NMR (400 MHz, Chloroform-d) δ 8.55 (s, 1H), 7.62 (d, J = 8.1 Hz, 1H), 7.57 – 7.48 (m, 3H), 7.35 – 7.23 (m, 6H), 7.19 – 7.05 (m, 7H), 4.42 (q, J = 7.2 Hz, 2H), 1.42 (t, J = 7.1 Hz, 3H). ¹³C NMR (101 MHz, Chloroform-d) δ 163.27, 148.51, 147.07, 130.09, 129.75, 129.45, 127.96, 125.12, 123.76, 123.02, 122.62, 113.69, 61.91, 14.26. ESI-MS (ESI) m/z calculated for C₃₀H₂₃NO₄ [M]⁺ 461.16, found [M+H]⁺ 462.17.

1.3.3 General preparation of compound 3

The solution of compound 2 (4.61 g, 10 mmol) in EtOH (15 mL) was added 15 mL of 10% NaOH and heated under reflux for 20 min. Acidification to pH 2 using concentrated hydrochloric acid and cooling to 0 °C gave an orange crystalline deposit (3.68 g, 85%). ¹H NMR (400 MHz, Chloroform-d) δ 8.92 (s, 1H), 7.75 (d, J = 8.2 Hz, 1H), 7.67 (d, J = 8.4 Hz, 1H), 7.63 (s, 1H), 7.53 (d, J = 8.5 Hz, 2H), 7.31 (t, J = 7.7 Hz, 4H), 7.18 – 7.08 (m, 8H). ¹³C NMR (101 MHz, CDCl₃) δ 184.64, 151.04, 130.69, 130.09, 129.52, 128.11, 125.32, 124.26, 124.05, 122.26, 113.79. ESI-MS (ESI) m/z calculated for C₂₈H₁₉NO₄ [M]⁺ 433.13, found [M-H]⁺ 432.13.

1.3.4 General preparation of TPACP and TPACP@Cu NPs

The solution of compound 3 (4.33 g, 10 mmol) in dichloromethane (100 mL) were added 1-Ethyl-3-(3-dimethylaminopropyl)carbodiimide hydrochloride (EDCI) (1.91 g, 10 mmol), 2-(aminomethyl)pyridine (1.08 g, 10 mmol), and a catalytic amount of 4-(dimethylamino)pyridine (DMAP) (120 mg, 1 mmol). The mixture was stirred for 8 h at room temperature. After the reaction is completed, the mixture was washed with water (3 × 50 mL) and dried over anhydrous sodium sulfate, and the solvent was removed

in vacuo. The crude product was further purified by column chromatography on alumina (eluant: ethyl acetate: Petroleum ether, 1:2 v/v) to afford a yellow solid (3.14 g, 60%). ¹H NMR (400 MHz, Chloroform-d) δ 9.63 (s, 1H), 8.91 (s, 1H), 8.63 (d, J = 4.8 Hz, 1H), 7.84 (s, 1H), 7.69 (d, J = 8.3 Hz, 1H), 7.58 (d, J = 8.1 Hz, 2H), 7.51 (d, J = 8.5 Hz, 3H), 7.36 (s, 1H), 7.27 (d, J = 17.6 Hz, 6H), 7.19 – 7.04 (m, 6H), 4.93 (d, J = 5.5 Hz, 2H). ¹³C NMR (101 MHz, Chloroform-d) δ 161.99, 149.44, 148.15, 147.07, 136.74, 130.04, 129.45, 127.99, 125.11, 123.75, 123.47, 122.64, 122.31, 121.69, 113.59, 45.38. ESI-MS (ESI) m/z calculated for C₃₄H₂₅NO₃₃ [M]⁺ 523.19, found [M+H]⁺ 524.19.

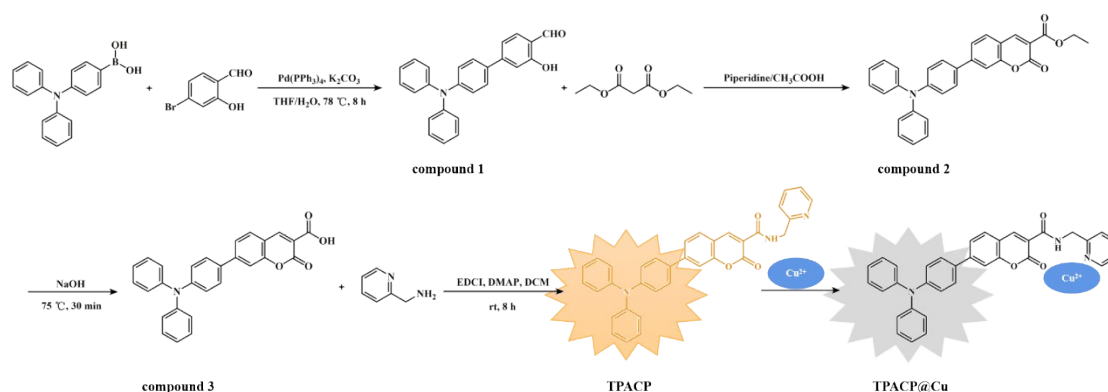
The TPACP@Cu NPs were prepared via the following procedure. In brief, 52.3 mg TPACP probe was dissolved in a mixture of 10 mL DMSO and H₂O (DMSO:H₂O) 1:9, v/v) to prepare a 10 mM TPACP stock solution. Next, 10 mM of copper nitrate solution was prepared in water. Then the 10 mM copper nitrate solution was slowly added to the TPACP solution until the fluorescence of TPACP was completely quenched. The initial solution after complexing Cu²⁺ was concentrated by evaporator at 60 °C. When the concentration reached a certain level, a precipitate would precipitate out. The precipitate is filtered out and washed several times with deionized water to remove the excess Cu²⁺. The resulting filter residue was then dried in a freeze dryer for 24 h to obtain tan colored nanoparticles (TPACP@Cu) that chelate Cu²⁺.

1.4 Cytotoxicity and cell imaging

The cytotoxicity of TPACP and TPACP@Cu NPs was evaluated by a standard cell counting kit-8 (CCK-8) assay. The cell line was obtained from the Cell Resource Center, Peking Union Medical College (which is the headquarter of National Science & Technology Infrastructure-National Biomedical Cell-Line Resource, NSTI-BMCR). HeLa cells were inoculated in 96-well plates with a density of 5×10^3 cells/well, and Dulbeccos Modified Eagle Medium (DMEM) containing 10% fetal bovine serum. The cells were cultured in cell culture box for another 24 h until the cell fusion rate reached over 80% and completely adhered to the cell plates. Different concentrations of TPACP (5, 10, 20, 40, 80 and 160 μg/mL), TPACP@Cu NPs (10, 20, 40, 60, 80, 100 and 160 μg/mL) and TPACP@Cu NPs supplemented with additional H₂O₂ (20 μM and 40 μM) were incubated with HeLa cells separately for 24 h and CCK-8 solution (5 mg/mL) was added to each well. After 3 h, the absorbance of each well was determined at wavelength of 450 nm. The experiment was repeated three times and the cell viability and standard deviation were calculated by absorbance. The cells without incubation with TPACP and TPACP@Cu NPs were served as the control group. To evaluate the photodynamic activity of PDT, and the cells firstly

incubated with different concentrations of TPACP for 3 h and then the cells were irradiated with white light source (5 and 10 mW/cm²) for 3 min. After another 24 h incubation, same concentration of CCK-8 was added into cell plates. The cell viability was determined by the procedure as described above.

The cell uptake behavior of TPACP was investigated by confocal scanning microscope (CLSM, Zeiss LSM710 3-channel, Germany) using HeLa cells. HeLa cells were incubated with DMEM supplemented with 1% penicillin streptomycin and 10% fetal bovine serum under a humidified incubator at 37 °C, in 5% CO₂. HeLa cells were incubated with the probe TPACP (10 μM) in PBS buffer for 3 h. Afterward, cells were washed three times with PBS to remove TPA and then fixed with paraformaldehyde for 12 min. Fluorescence imaging of cells was taken by CLSM by using a 458 nm laser. To evaluate the detection of Cu²⁺ in living cells. The HeLa cells were incubated for TPACP (10 μM) for 3 h and then Cu²⁺ (final concentration is 10 μM) was added and incubated for another 20 min. Then the cells were then fixed with para-formaldehyde for 12 min. The CLSM images were obtained by excited with 458 nm laser and to evaluate the response of probe toward Cu²⁺. The production of reactive oxygen species in cells under light conditions was detected using DCFH-DA as an indicator. The cells were firstly inoculated in a 96-well plate with a cell density of 5000 cells for 24 h. The probe (20 μg/mL) was added to the cell culture dish and incubated under dark conditions for 3 h. The culture medium was removed and washed three times with PBS buffer to remove the remaining culture medium. Next, DCFH-DA (10 μM) was added to the culture medium and incubated for another 30 min. after that, the cells were irradiated for 5 min under a 450 nm laser with a light intensity of 20 mW/cm². Fluorescence images were captured by inverted fluorescence microscopy.



Scheme S1 The schematic illustration of proposed synthetic routes and chemical structure of TPACP and TPACP@Cu NPs.

2 Results

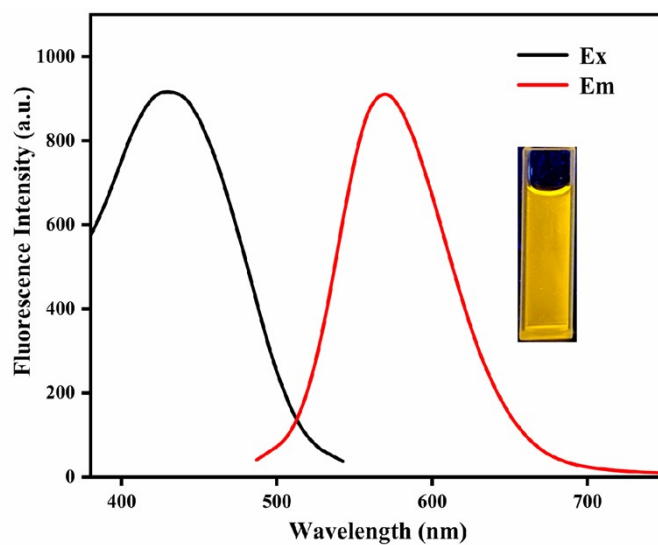


Fig. S1 The excitation and emission spectrum of TPACP in DMSO/H₂O (v/v is 1:9) mixture. The inset picture in Figure is the solution of TPACP under irradiation with UV lamp at 365 nm.

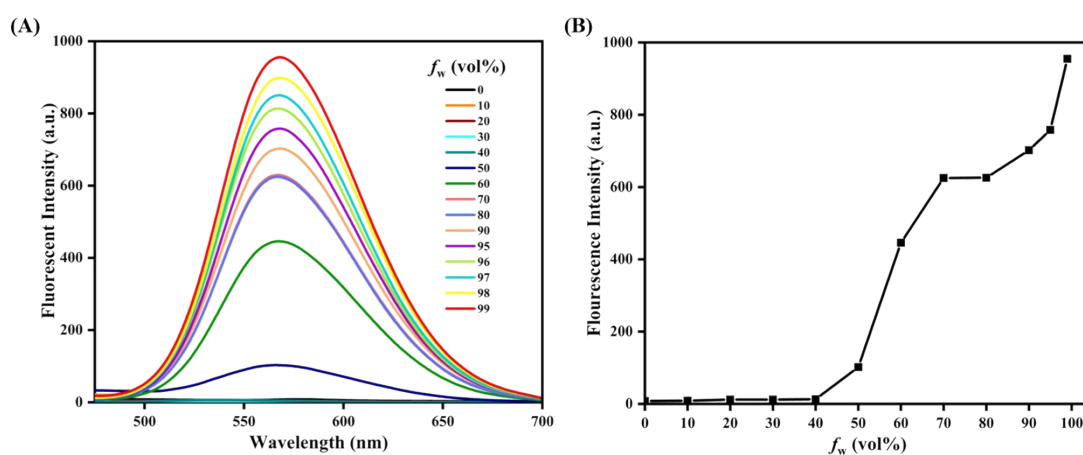


Fig. S2 (A) Emission spectrum of TPACP (30 μM) in DMSO/H₂O mixtures with different water volume fractions (f_w). (B) The relationship of fluorescence spectrum of TPACP versus water fraction in mixed solution

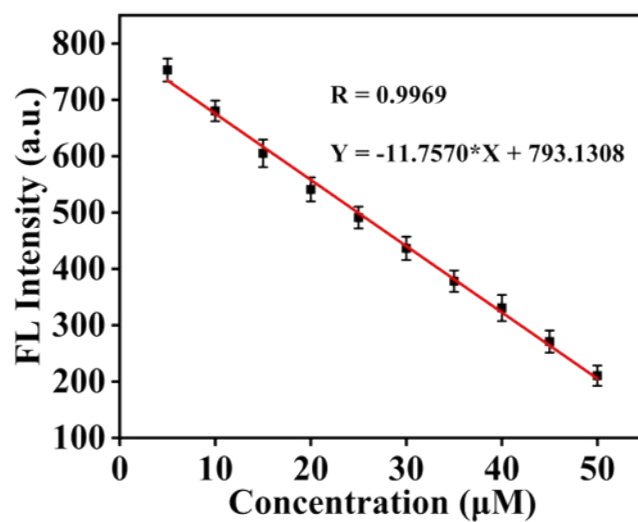


Fig. S3 A linear calibration curve between the fluorescent intensity and the concentration of Cu^{2+} .



Fig. S4 The fluorescence photographs of TPACP before and after adding Cu^{2+} in PBS buffer ((PBS:DMSO) 8:1, v/v) under 365 nm UV irradiation from a portable UV lamp and natural light.

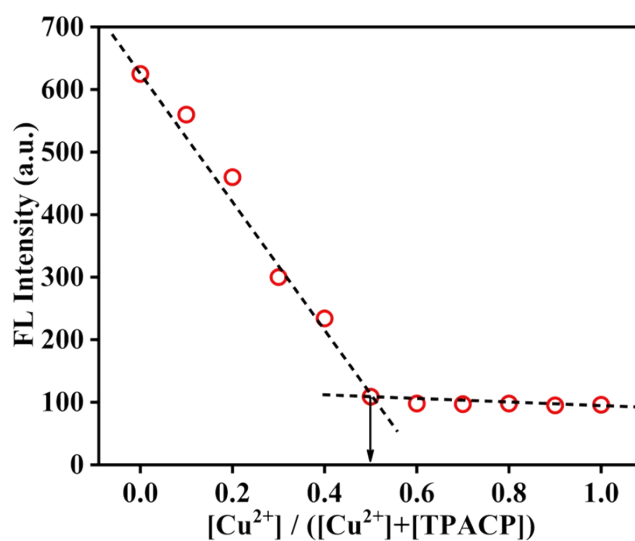


Fig. S5 Job's plot of TPACP vs. Cu^{2+} in aqueous solution (PBS:DMSO = 9:1, v/v) (1.0×10^{-5} M).

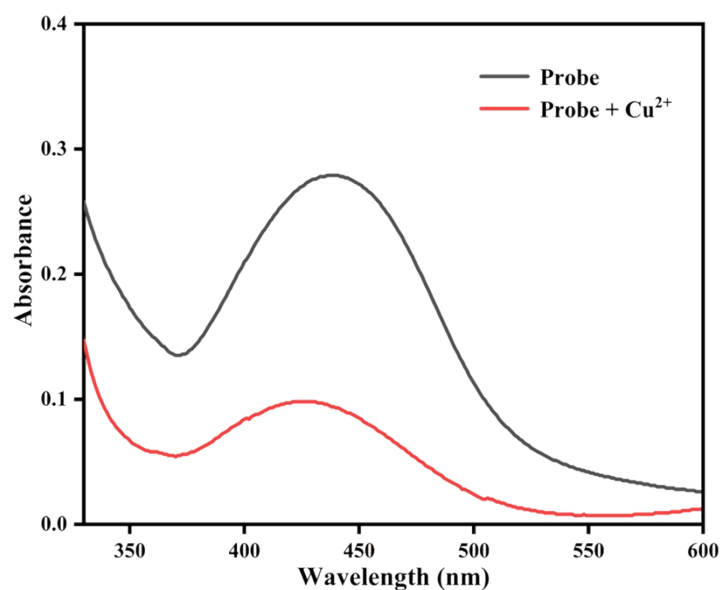


Fig. S6 The UV–Vis absorption spectrum of TPACP solution after adding Cu^{2+} in PBS buffer ((PBS:DMSO) 9:1, v/v).

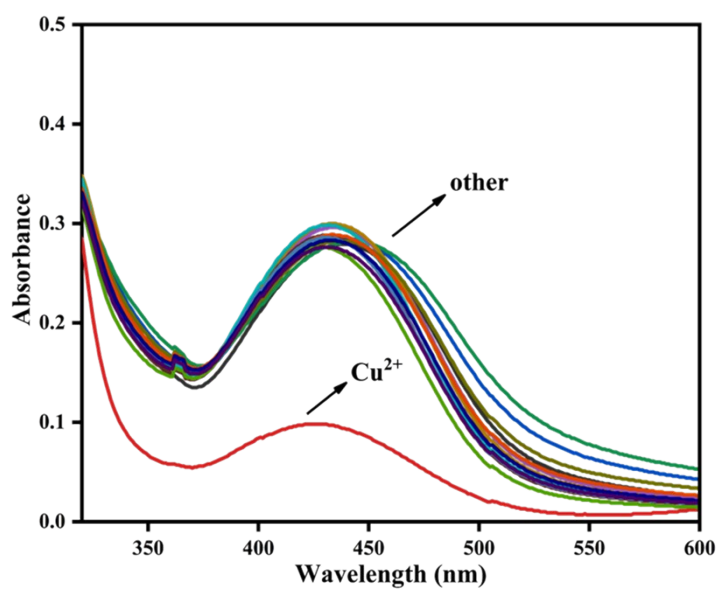


Fig. S7 The UV–Vis absorption spectrum of TPACP (30 μM) after adding 60 μM Cu^{2+} and other metal ions (Zn^{2+} , Mg^{2+} , Ca^{2+} , Fe^{2+} , Cr^{3+} , Co^{2+} , Al^{3+} , Ni^{2+} , Ag^+ , Pb^{2+} , Cs^+ , Na^+ , Hg^{2+}) in PBS (60 μM , pH 7.4).

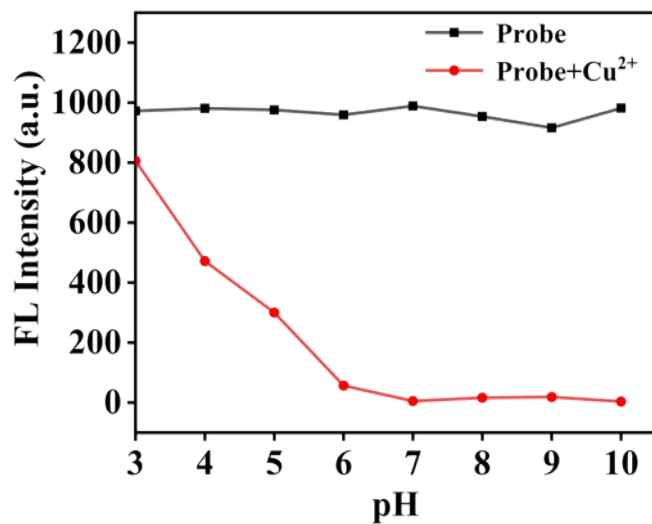


Fig. S8 The fluorescence intensity of TPACP at various pH values, the excitation wavelength was set at 440 nm.

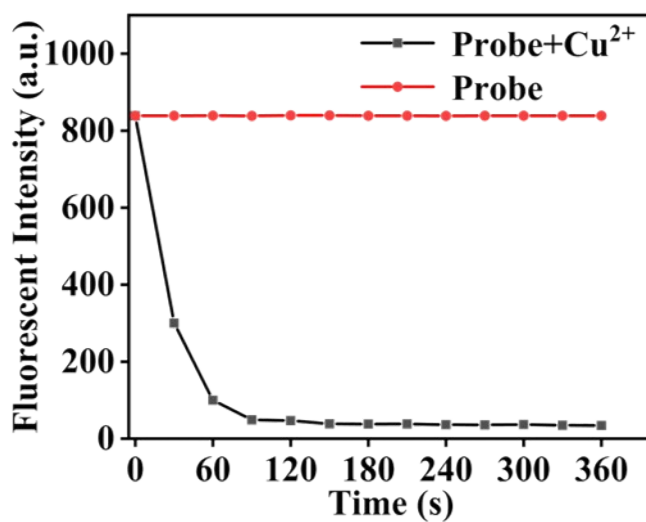


Fig. S9 The fluorescence intensity of TPACP as a function of reaction time.

Table S1 Comparison of fluorescent probes for detection of Cu²⁺

Probes	λ_{ex}	λ_{em}	LOD	Fluorescence Signal	AIE
BSP ²	367 nm	549 nm	59 μM	Turn-off	Yes
AIEgen-3 ³	362 nm	544 nm	24 nM	Turn-off	Yes

M201-DPA ⁴	373 nm	524 nm	88 nM	Turn-off	No
1-Cu ²⁺ ⁵	430 nm	479 nm	20 μM	Turn-off	No
1o ⁶	365 nm	588 nm	1.62 μM	colorimetric	No
HCD Probe 1 ⁷	400 nm	625 nm	0.44 μM	Turn-off	Yes
TPACP (This work)	440 nm	560 nm	0.19 μM	Turn-off	Yes

Firstly, the structures of TPACP and TPACP-Cu²⁺ complexes were optimized, and the molecular structure model of TPACP and Cu²⁺ coordination at a stoichiometric ratio of 1:1 was obtained. In the model, Cu²⁺ coordinated with the carbonyl group on coumarin, the N atom in amide, the N atom in pyridine, and two O atoms in water, respectively. The highest occupied molecular orbital (HOMO) and lowest unoccupied molecular orbital (LUMO) energy levels of TPACP and TPACP-Cu²⁺ complexes were also calculated. As can be seen from **Fig. S10**, the energy gap between HOMO (-5.01 eV) and LUMO (-2.27 eV) levels of TPACP is 2.74 eV. However, the energy gap between HOMO (-5.02 eV) and LUMO (-2.80 eV) levels of TPACP-Cu²⁺ complexes was reduced to 2.22 eV after adding Cu²⁺, indicating that TPACP and Cu²⁺ formed a stable TPACP-Cu²⁺ complexes. In addition, HOMO of TPACP is mainly distributed in TPA and part of coumarin moiety, and LUMO is mainly distributed in coumarin backbone. However, when Cu²⁺ is coordinated with TPACP, LUMO of TPACP-Cu²⁺ is mainly concentrated on Cu²⁺. The above analysis suggests that upon binding of TPACP with Cu²⁺, electrons are transferred from excited TPA moiety to Cu²⁺ moiety, resulting in fluorescence quenching. This mechanism provides a route for nonradiative deactivation of excited states. The charge transfer results obtained in computational simulations of TPACP-Cu²⁺ complexes are consistent with presumed results from fluorescence spectral data, so it is inferred that fluorescence quenching mechanism of probe in the presence of Cu²⁺ is attributed to LMCT mechanism.

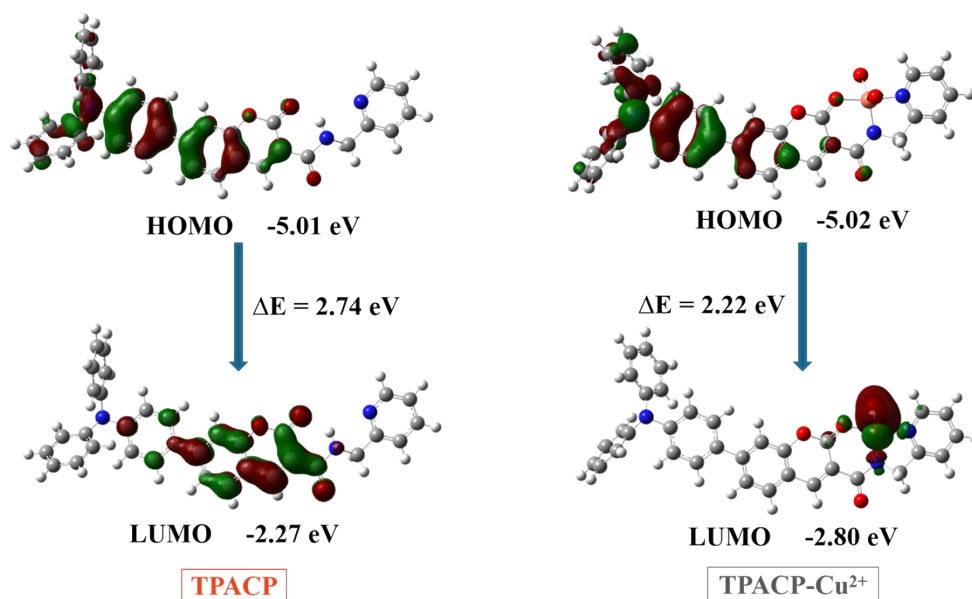


Fig. S10 Highest occupied molecular orbital (HOMO) and lowest unoccupied molecular orbital (LUMO) distributions calculated at the B3LYP with 6-31G* basis, showing the possible charge transfer direction changes.

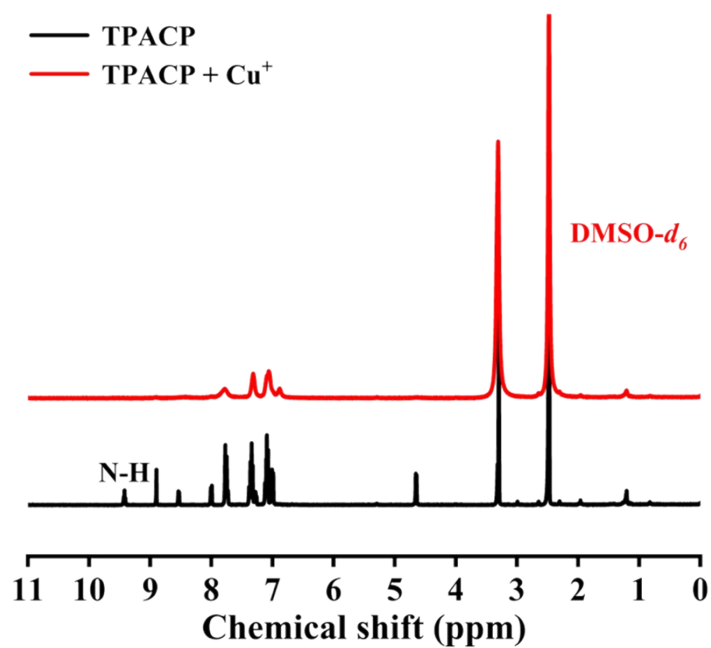


Fig. S11 ¹H NMR spectrum of TPACP in the absence and presence of Cu⁺.

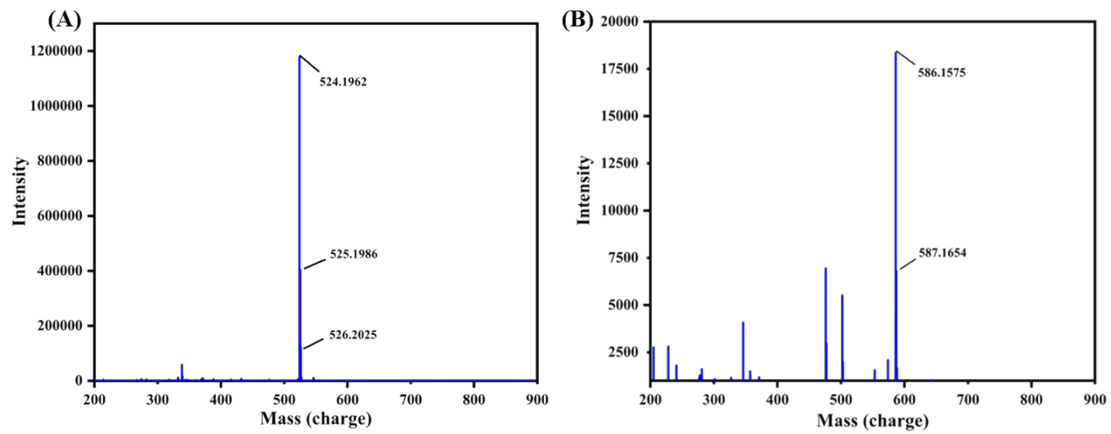


Fig. S12 ESI-MS data of (A) TPACP and (B) TPACP-Cu²⁺.

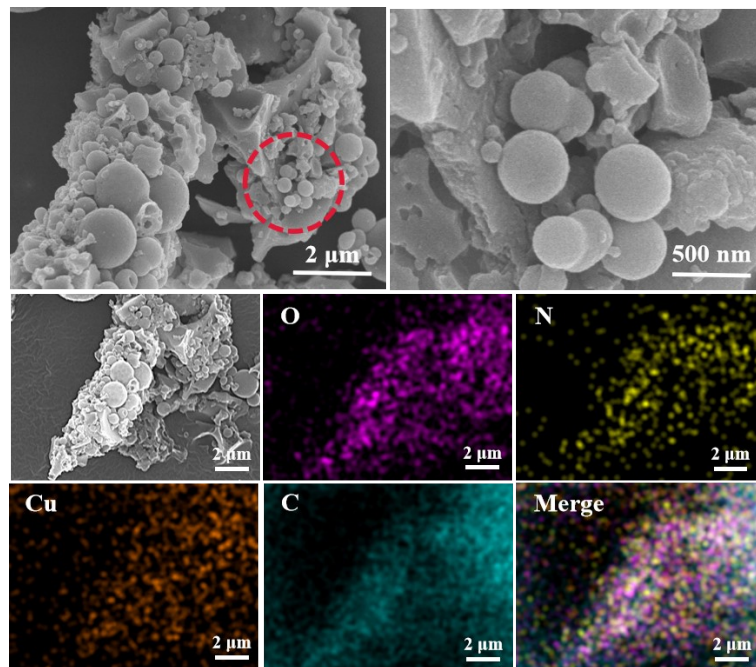


Fig. S13 The SEM/EDS mapping images of TPACP@Cu NPs.

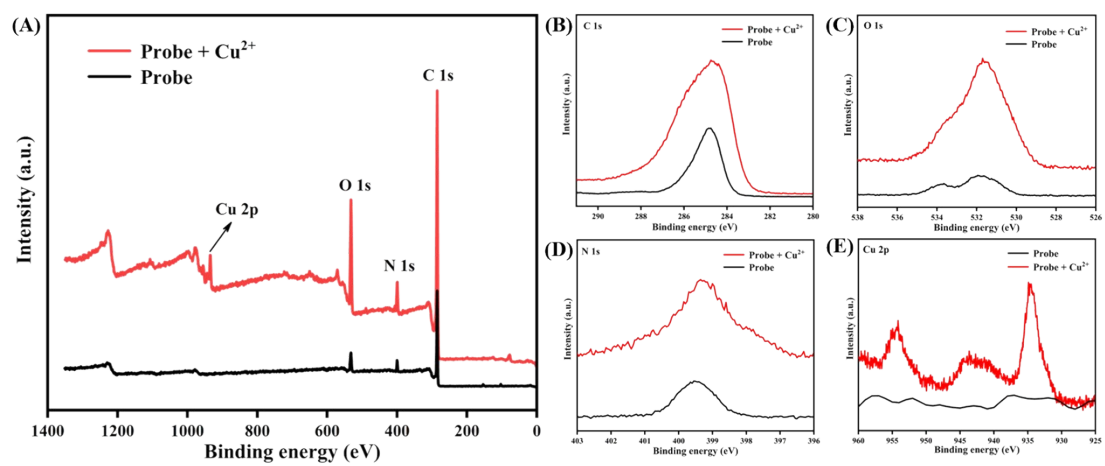


Fig. S14 XPS spectra of TPACP and TPACP@Cu NPs. (A) survey XPS spectra (B) high resolution of C 1s region; (C) high resolution of O 1s region; (D) high resolution of N 1s region; (E) high resolution of Cu 2p region.

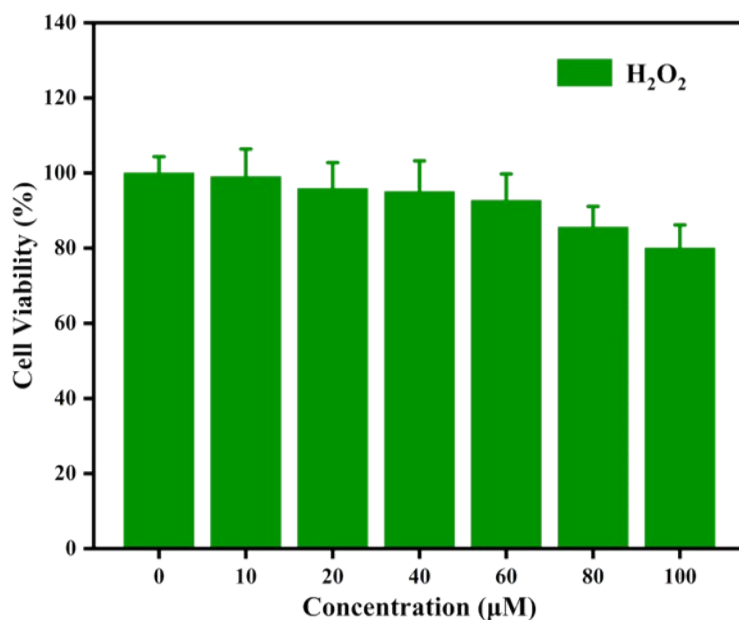


Fig. S15 The cell viability of HeLa cells after incubated with different concentrations of H₂O₂ for 24 h.

No.	Reaction
1	$\text{Cu}^{2+} + 2\text{GSH} \rightarrow \text{Cu}^+ + \text{GSSG}$
2	$\text{Cu}^{2+} + \text{H}_2\text{O}_2 \rightarrow \text{Cu}^+ + \text{HO}_2^- + \text{H}^+$
3	$\text{Cu}^+ + \text{H}_2\text{O}_2 \rightarrow \text{Cu}^{2+} + \text{OH}^- + \text{OH}\cdot$

Fig. S16 Mechanism of Fenton or Fenton-like reactions in living organisms.

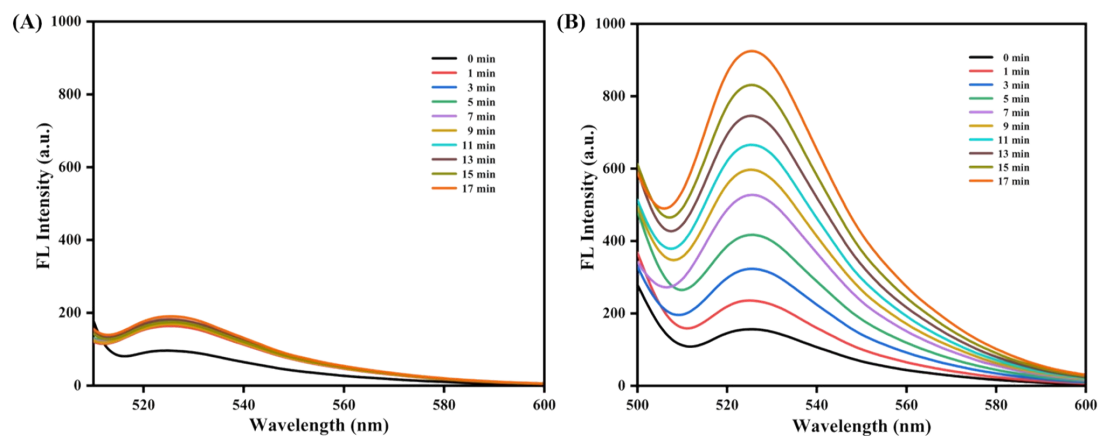


Fig. S17 Fluorescence spectra of the DCFH-DA ($1 \mu\text{M}$, 4 mL) in the presence of $10 \mu\text{L}$ TPACP ($200 \mu\text{g/mL}$) under irradiation with different time points (A) Blank, (B) TPACP.

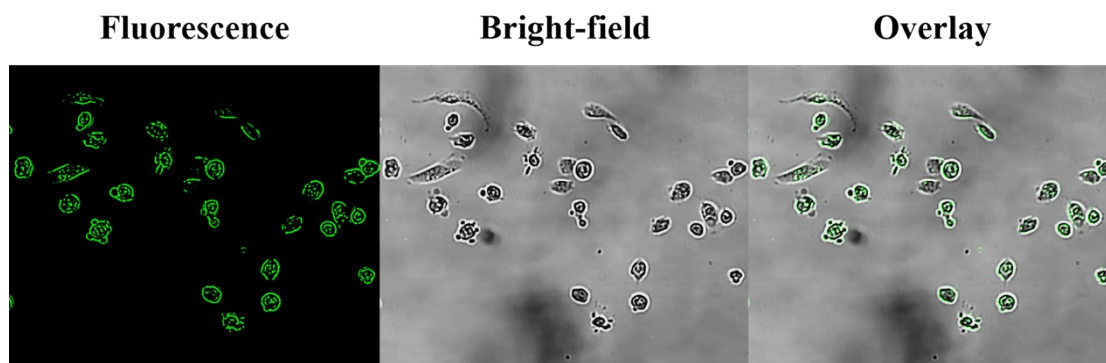


Fig. S18 General ROS generation of TPACP ($20 \mu\text{g mL}^{-1}$) in U2OS cells under light irradiation (20 mW/cm^2) by using DCFH-DA ($10 \mu\text{M}$).

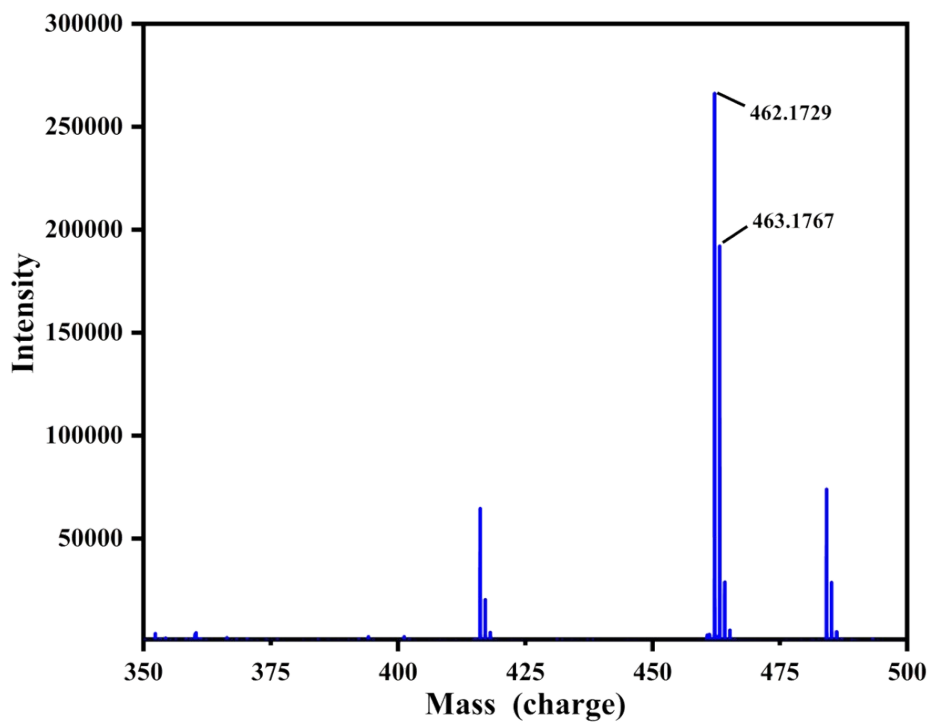


Fig. S21 ESI-MS data of compound 2.

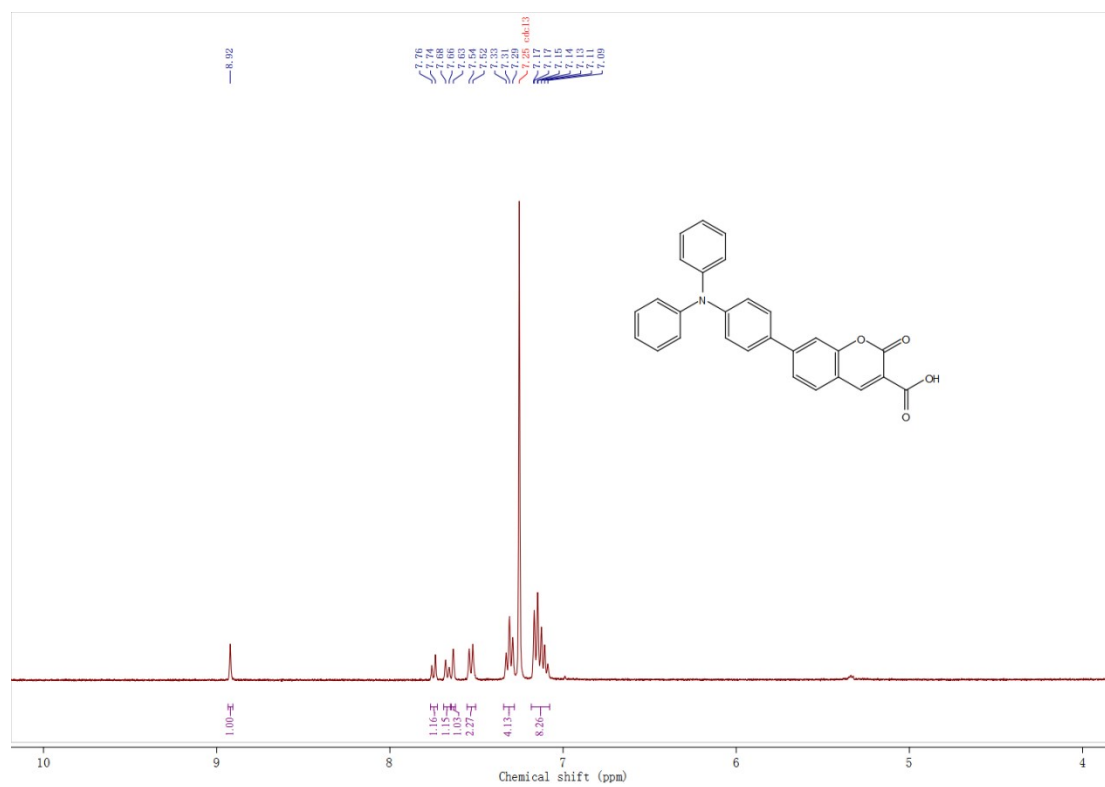


Fig. S22 ¹H-NMR spectrum of compound 3 in chloroform-*d*.

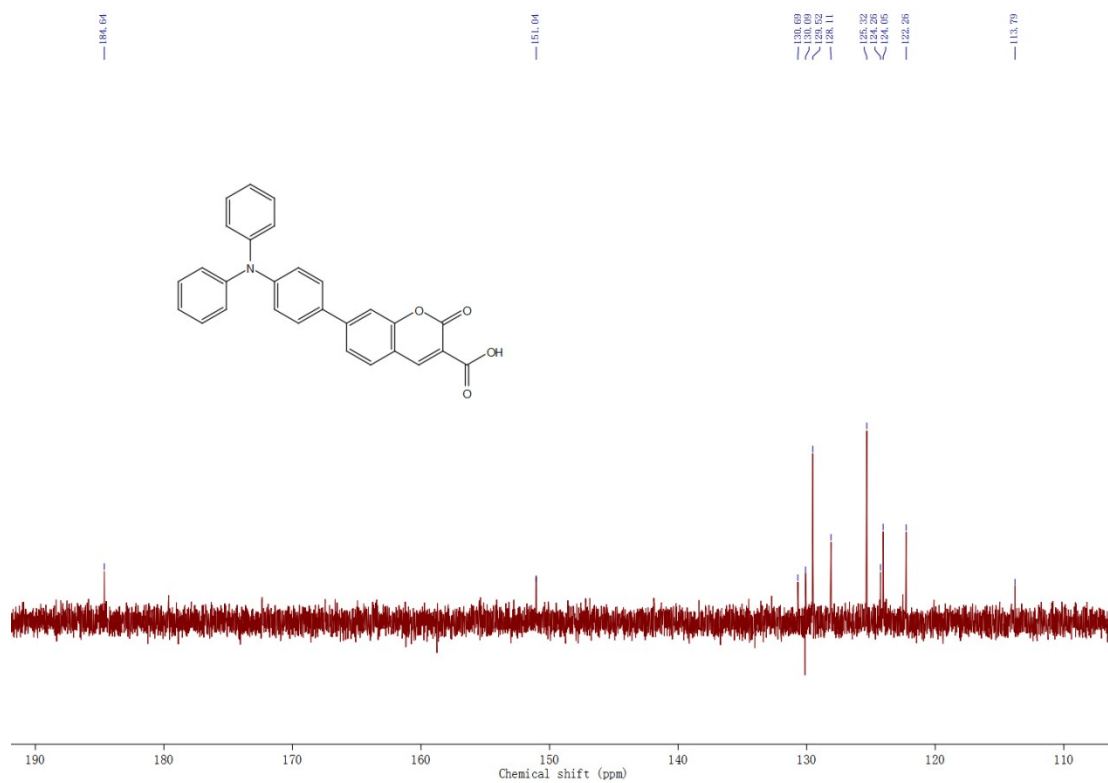


Fig. S23 ^{13}C -NMR spectrum of compound 3 in chloroform-*d*.

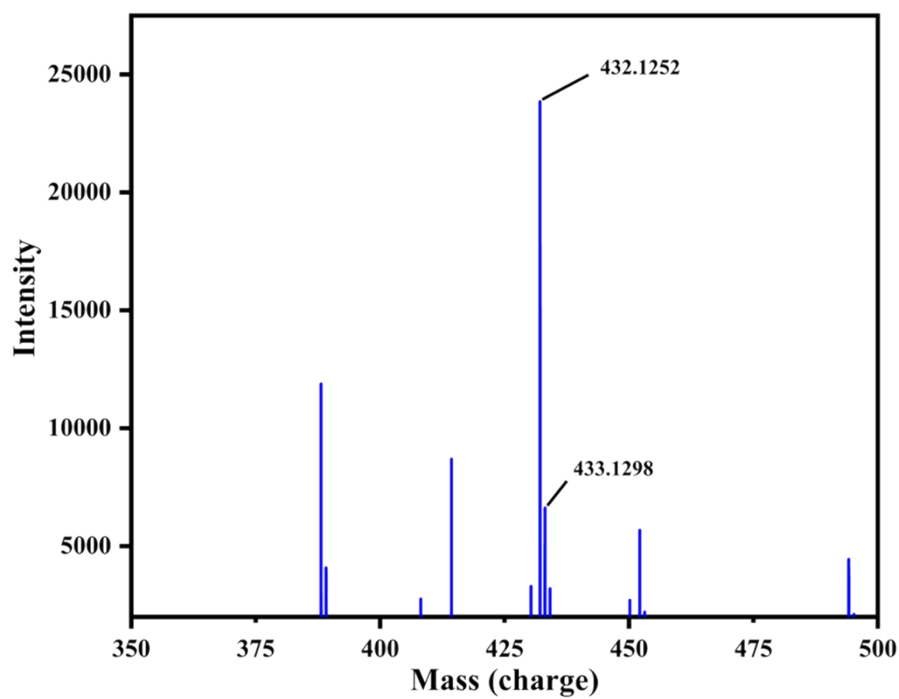


Fig. S24 ESI-MS data of compound 3.

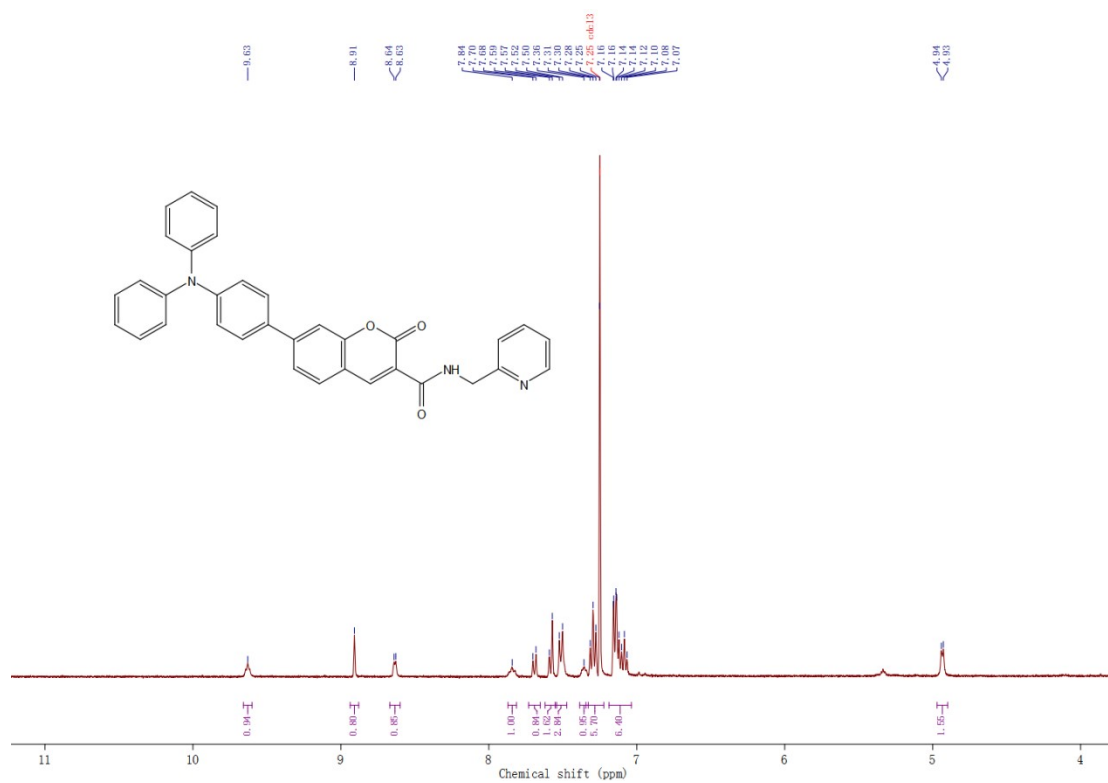


Fig. S25 ¹H NMR spectrum of compound 4 in chloroform-*d*.

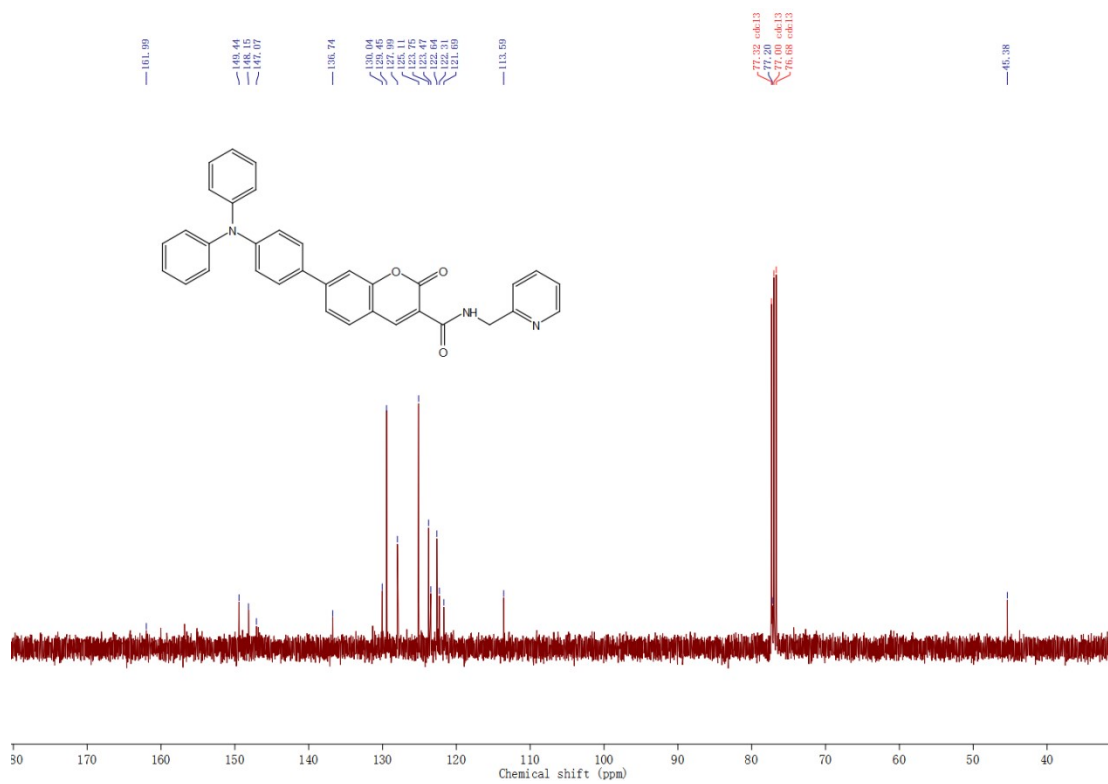


Fig. S26 ¹³C-NMR spectrum of compound 4 in chloroform-*d*.

References

- 1 J. Fu, X. Hu, Y. Liang, T. Guo, F. Deng, W. Zhu, M. Liu, Y. Wen, X. Zhang and Y. Wei, *Dyes Pigm.*, 2022, **207**, 110764.
- 2 N. Miengmern, A. Koonwong, S. Sriyab, A. Suramitr, R. P. Poo-arporn, S. Hannongbua and S. Suramitr, *J. Lumin.*, 2019, **210**, 493-500.
- 3 S. K. Padhan, N. Murmu, S. Mahapatra, M. K. Dalai and S. N. Sahu, *Materials Chemistry Frontiers*, 2019, **3**, 2437-2447.
- 4 S. Sakunkaewkasem, A. Petdum, W. Panchan, J. Sirirak, A. Charoenpanich, T. Sooksimuang and N. Wanichacheva, *ACS Sensors*, 2018, **3**, 1016-1023.
- 5 H. S. Jung, P. S. Kwon, J. W. Lee, J. I. Kim, C. S. Hong, J. W. Kim, S. Yan, J. Y. Lee, J. H. Lee, T. Joo and J. S. Kim, *J. Am. Chem. Soc.*, 2009, **131**, 2008-2012.
- 6 S. Cui, S. Pu and Y. Dai, *Anal. Methods*, 2015, **7**, 3593-3599.
- 7 M. A. Assiri, A. G. Al-Sehemi and M. Pannipara, *Inorg. Chem. Commun.*, 2019, **99**, 11-15.